Serbian Tribology Society

SERBIATRIB '19

16th International Conference on Tribology

Faculty of Engineering University of Kragujevac

Kragujevac, Serbia, 15 – 17 May 2019

FABRICATION OF SILICON CARBIDE REINFORCED ALUMINIUM FOAMS USING FRICTION STIR PROCESSING ROUTE

Ioannis PAPANTONIOU[1], Nikolaos VAXEVANIDIS[2,*], Dimitrios MANOLAKOS[1]

[1] Laboratory of Manufacturing Technology, School of Mechanical Engineering, National Technical University of Athens, 9 Heroon Polytechniou Street, 15780, Zografos, Greece

[2]Laboratory of Manufacturing Processes and Machine Tools (LMProMaT), School of Paedagogical and Technological Education, (ASPETE), Greece

*Corresponding author: vaxev@aspete.gr

Abstract: *Microcellular materials and specifically metallic foams have attracted the attention of scientific community due to the advanced combination of particular properties that they offer, compared to solid metals. These combined properties make them revolutionary materials for applications requiring more than one function such as high stiffness, fire protection and sound insulation. The present research focuses on the development of a method of producing composite metallic foam localized regions on metallic parts using a friction stir processing route (FSP). This route consists of friction stir processing passes for the integration of the foaming and the stabilizing/reinforcing agents in the aluminium matrix (precursor specimens) and a separate foaming stage at a laboratory furnace. More specifically, a mix of microsized particles of silicon carbide (stabilizing/reinforcing agent) and titanium hydride (foaming agent) were dispersed on bulk aluminium alloy AA5083–H111 using FSP. The integration of the mix was achieved via grooves which were constructed along the plate, parallel to the rolling direction. The parameters investigated during the experimental procedure were the groove geometry and the number of FSP passes. The analysed outcomes were the dispersion of carbide particles in the stir zone of the precursor and the porous structure and morphology of the composite foamed aluminium. The results were correlated with hardness evolution in both precursor and final foamed specimens.*

Keywords: *Friction Stir Processing, porous materials, aluminium foams, composite metal matrix foams, silicon carbide, localized foamed structures.*

1. INTRODUCTION

The highly increasing demand for lightweight and at the same time high strength materials suitable for automotive, railway, aerospace and shipbuilding industries resulted in the growth of research and industrial applications of different type of hybrid materials. Cellular and microcellular materials are among a new class of hybrid materials and are found in everyday uses. Applications range from light-weight construction and packaging to thermal insulation, vibration damping, and chemical filtration [1]. Metallic cellular materials, namely metal foams, merit the use of cellular materials and are becoming a new very promising class of engineering materials. Metal foams offer unique properties, compared to solid metals. Such unique properties are their high strength to weight ratio, high energy absorption capacity, large specific surface, high gas and liquid permeability, and low thermal conductivity [2]. Thus, metallic foams can be used as single elements, as a core of sandwich panels, as filler materials of hollow structures in multi-functional hybrid construction elements, for energy absorption, sound absorption, vibration damping and heat dissipation [3].

The use of metal foams depends on their basic characteristics such as porosity, cell structure and cell morphology homogeneity [4]. Metal foams are expected to be used as components in automotive, aerospace and marine industries, where the large strength and stiffness to weight ratios and the safety are crucial issues [5,6].

Friction stir process (FSP) is a surface modifying technique which involves the generation of friction heat and intense plastic flow. During FSP a rotating tool with pin and shoulder is inserted in a single piece of material for microstructural modification and traversed along the desired line to cover the region of interest. FSP was developed from the basic principles of friction stir welding (FSW), which is a solid-state bonding process [7,8]. The FSP has been used for fabricating metal matrix composites with uniformly dispersed reinforcing particles owing to its high mixing ability [9-11].

Hangai et al. [12,13] introduced the application of FSP for manufacturing aluminum foams. The proposed method utilized FSP on AA1050 and AA4045 to produce precursor specimens. Firstly, two aluminum plates were stacked with the blowing agent and the stabilizing agent between the plates. Then, FSP passes were carried out to mix the mixture of blowing and stabilization agent into the aluminum plates and to create precursors which were heat treated afterward at a separate foaming process. Papantoniou et al. manufactured AA5083/nano-γAl_2O_3 [14] and AA5083/ MWCNT [15] reinforced composite foams at localized regions using a novel single aluminium plate process.

The main goal of the present study was to produce silicon carbide reinforced Al-foam regions on a single AA5083 plate. The silicon carbide microsized particles aimed to reinforce and to stabilize the porous structure of the final composite foam. Process parameters in this paper have been set with the intention to find a correlation among the composite metal foam foaming process, the microstructure evolution and the hardness distribution.

2. MATERIALS AND METHODS

2.1 Materials

The selected base metal was the AA5083-H111 in plates of 6 mm thickness. The selection of the specific alloy was due to two significant reasons: i) firstly the AA5083 is a not-heat treatable alloy; thus the mechanical properties after the FSP are not degraded [14], ii) secondly the high presence of the alloying element magnesium is expected to improve the wetting of the reinforcing particles [16]. Microsized Silicon carbide particles (Alfa Aesar, 325 mesh, 99.5%) were used as reinforcing and stabilizing material. Commercially available titanium hydride powder (with particle diameter < 45 μm) was used as a blowing agent.

2.2 FSP based manufacturing procedure

Friction stir processing experiments were carried out using a modified milling machine. The FSW tool was made of heat-treated steel; it consisted of a flat shoulder and a cylindrical threaded pin. The diameter of the shoulder was 22.19 mm, the diameter of the pin was 5mm and its height was 4.2 mm. The height of the pin determines the thickness of the layer that will be enhanced with the ceramic and the foaming particles.

Initially, FSP tests were carried out without any addition of reinforcing particles in order to define the optimum parameters that result in a defect-free stir zone, consisted of good material mixing and refined microstructure. The optimum adopted operational FSP parameters for the precursor specimens without nanoparticle reinforcement resulted from preliminary experiments that their presentation beyond of the scope of this paper. These experiments indicated the requisition for applicability of 1000 rpm rotational speed combined with 13 mm/min transverse speed.

The first stage of the manufacturing procedure was the machining of the grooves (Figure 1i). The grooves were machined parallel to the rolling direction of the plates and were aligned with the center line of the rotating pin.

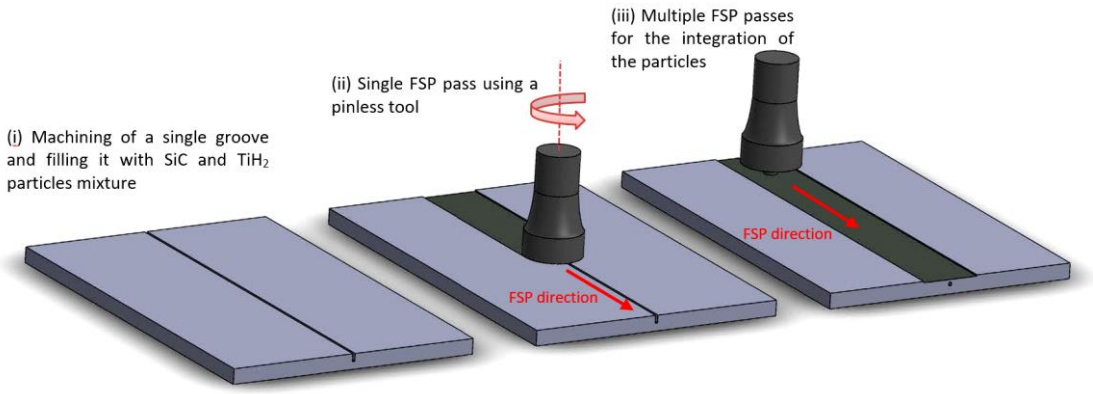

Figure 1. Precursor FSP manufacturing process

Two groove geometries have been used during the present study. The first geometry had a cross section of 1 mm width and 2.9 mm depth whether the second geometry had a cross section of 1 mm width with 3.9 mm depth.

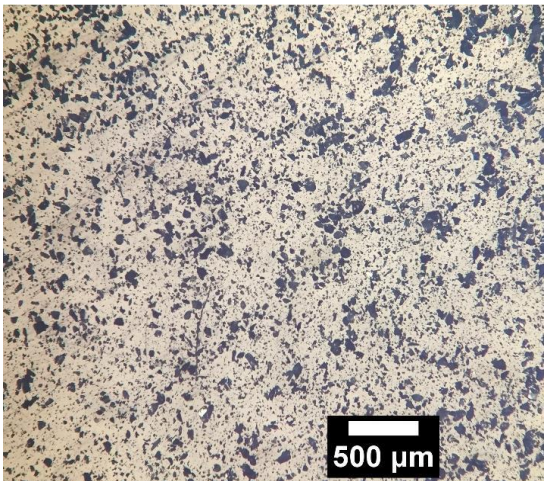

Figure 2. Micrograph (dark-field) of TiH_2 and SiC particles after the powder mixing stage

The precursor specimens were manufactured by mixing blowing agent powder (0.6% w/w TiH_2) and reinforcing/stabilizing silicon carbide microsized particles (4.0% w/w SiC) (Figure 2). The mixture of TiH_2 and SiC particles was firstly mixed for thirty minutes in a powder mixer and was then inserted carefully in the grooves and was pressed down, so as to fill them in a uniform manner.

To prevent ejection of the powder during the process, the groove was initially covered, using a pinless tool, by a single FSP pass (Figure 1ii). After covering the groove, multiple passes were carried out sequentially in the same direction and in such a way so as not to allow samples to cool down to room temperature between the passes (Figure 1iii). According to literature, increasing the number of FSP passes results in a more uniform nanoparticle distribution in the nugget [17]. Two, three, five and eight FSP passes were performed for each groove geometry.

2.3 Foaming Process

All the precursor samples were thermally treated in a preheated electric inductive oven, at a temperature range above liquidus, to induce the foaming process. The samples were held at a temperature of 750°C for five minutes. After the foaming process, the foamed specimens were air cooled to room temperature. An especially designed setup was used to characterize the free expansion behavior of the specimens during the foaming stage. The setup consisted of a ceramic-glass window at the front side of the furnace and a high definition camera mounted at a close distance behind the glass. The camera was connected to a computer for recording images. Using this setup, we were able to monitor the foaming process in all the experiments. The foaming time used was five minutes in order to observe all the foaming stages (growth, peak, coarsening and decay). Due to the fact that the porous structure was at localized regions; the calculation of the foaming efficiency of the foamed areas needed a different approach. Thus, for the estimation of the foaming efficiency, the specimen thickness increment corresponding to the initial specimen thickness was calculated by

analysing the images from the camera using the open-source image processing software ImageJ (Figure 3).

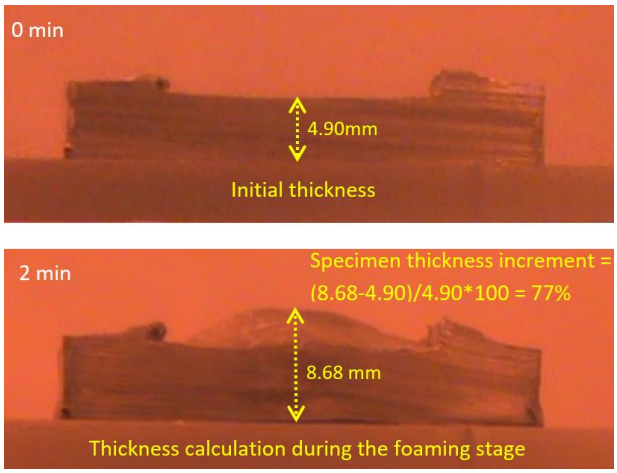

Figure 3. Specimen thickness increment calculation during the foaming stage (foaming efficiency estimation)

2.4 Metallurgical inspection

Specimens were created at different typical foaming times (e.g. peak, decay) in order to examine the porous structure. Cross-sections of the specimens were cut using a cut-off machine and processed by Electro Discharge Machining (EDM) to visualize the interior structure, without introducing any smearing effects in the porous structure.

Precursor specimens and foamed samples from each set of the experiment were polished with a suspension of 0.05 µm colloidal silica and then etched. Finally, the specimens were examined macroscopically by using a Leica MZ6 optical stereoscope, while microscopic observations were carried out by the optical microscope Leica DMILM.

2.5 Large-Scale Specimen

After obtaining the parameters that resulted in the optimum foamed specimen, a large-scale specimen was manufactured and analysed. For the manufacturing of the specimen, three grooves were machined in parallel and in close distance so as the stir-zones to be consecutive but not overlapped. Metallurgical inspection was also performed in this specimen and the microstructural observations were correlated to hardness distribution for both precursor and foamed specimens.

3. RESULTS AND DISCUSSION

3.1 Foaming Efficiency Results

Figure 4 illustrates the specimen thickness increment diagram (which is linked to the foaming efficiency) combined for all the specimens. From the diagram the following remarks were drawn. Firstly, it should be noted that the specimens with the two FSP passes introduced the lowest foaming efficiency. This correlates with the qualitative results obtained from the metallographic analysis of the cross-section of the precursor specimen in both specimens with different groove depths. Figure 5 illustrates stereoscopic images of the etched stir-zones of the two FSP passes precursor specimens. The ceramic particles were not found to be well distributed in the stir zones and large agglomerated areas in the center of the nuggets can be identified.

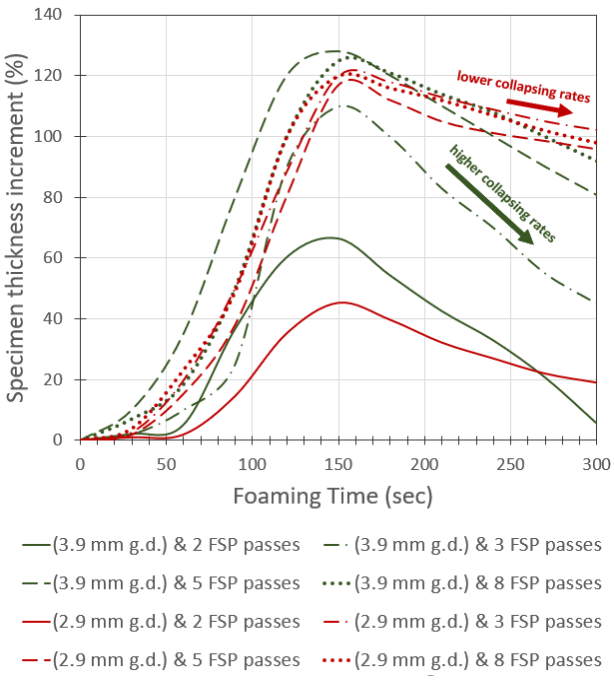

Figure 4. Specimen thickness increment-time diagram for different set of parameters during the foaming stage (g.d.: grooves depth)

The maximum foaming efficiency for all the other specimens was found to be in close values, even though the specimens with the larger groove depth had higher amounts of

foaming TiH_2 particles due to the larger groove volume. The important outcome of this diagram is that the specimens with the deeper groove introduced a higher rate of collapsing than the specimens with the shorter groove. This can be attributed to the higher amount of the hard silicon carbide particles on the deeper groove that were not uniformly dispersed in the nugget during the FSP passes. This can be observed also from the stereoscopic image of Figure 6 where the higher volume groove introduced a non-uniform stir-zone with many areas of agglomerated particles. The deficiency of stabilizing agents led to higher collapsing rates.

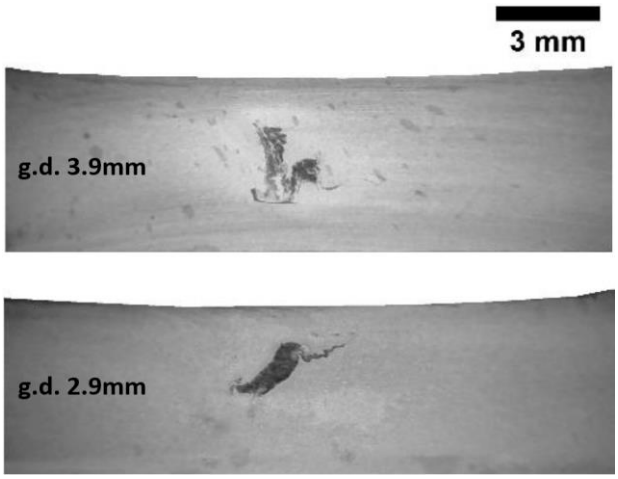

Figure 5. Macrographs of the cross-section of the specimens with 2 FSP passes for the two different groove depths

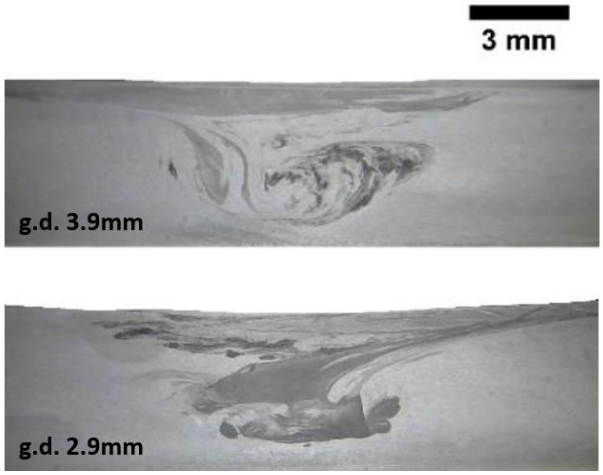

Figure 6. Macrographs of the cross-section of the specimens with 8 FSP passes for the two different groove depths

3.2 Large-Scale Specimen Results

For the large-scale specimen, three parallel grooves using the lower volume groove geometry were manufactured. Three FSP passes for each groove were chosen firstly due to the research outcome that for two and higher FSP passes the foaming efficiency was found to stay stable (Figure 4) and secondly for applicability reasons of the process. Figure 7a illustrates large scale specimens foamed at different foaming times. At the first specimen the foam has finished the nucleation and growth stage and has reached its peak. At the second and the third specimen the pores have started to coarse and merge and the structure gradually collapses and decays. Figure 7b shows the cross-section of the precursor specimen.

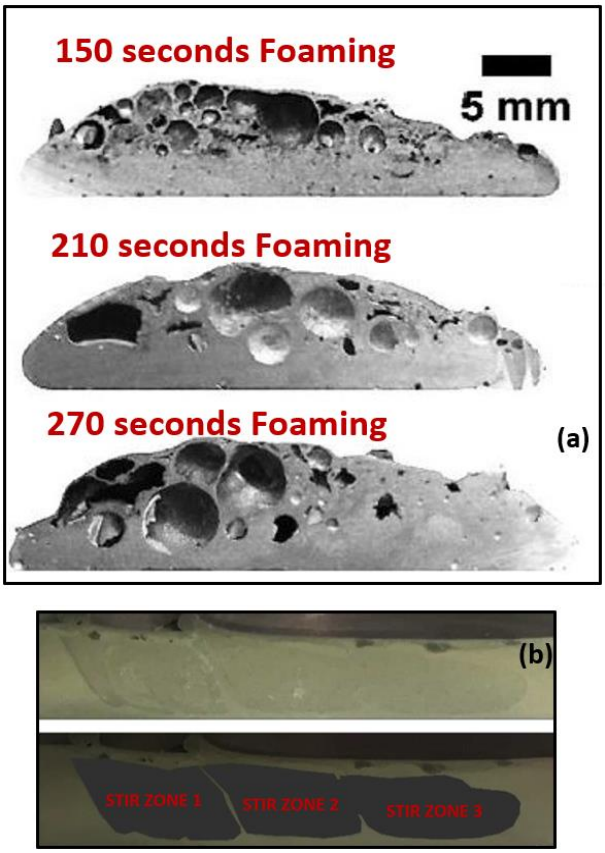

Figure 7. Large-Scale Specimens: a) Foamed specimens at different foaming times/stages (nucleation-growth-peak, coarsening, decay), b) Macrograph of precursor cross-section

Figure 9 illustrates optical microscopy images (dark field) of different regions of the large-scale precursor specimen. The distribution of the silicon carbide particles inside the stir zone appears to be totally homogeneous without introducing large agglomeration areas. On the foamed specimens the foam structure presented non-interconnected cellular morphology as it

was expected and the foamed samples were characterized by dense strut and close-packed grains on the cell wall surface. The silicon carbide particles remained well distributed in the foamed matrix (Figure 10a-b) enhancing the stabilizing and reinforcing of the foamed region. Furthermore, on the ligament regions, most of the particles appear to protrude on the solid-air interfaces (indicated with red arrows in Figure 10b). The micrographs from the etched foamed specimen illustrated struts with a dendritic, relatively coarse-grained microstructure (Figure 10b-c).

The hardness evaluation of the large-scale foamed specimen, across the perpendicular axis of friction stir process, revealed a mean value of hardness evolution about 85-87 HV outside the stir-zone and inside the stir-zone the values fluctuated from 119 to 126 HV (Figure 8a).

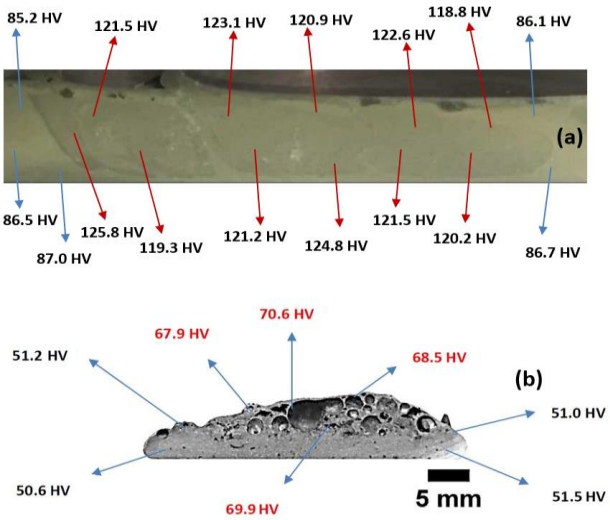

Figure 8. Variation of the hardness distribution along the cross section of: a) the FSPed precursor specimen, b) the foamed (at its peak) specimen

The increase is attributed to the presence of the hard microsized silicon carbide particles and to the Orowan mechanism where silicon carbide particles act as barriers.

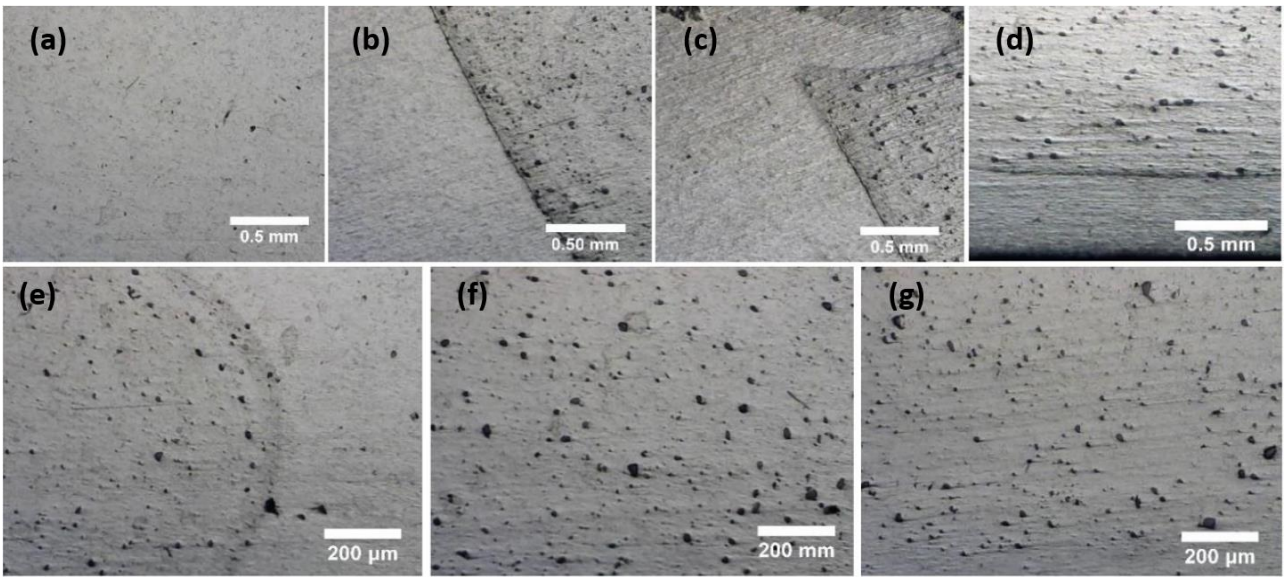

Figure 9. Optical microscopy (dark field) images of the precursor specimen on different regions: a) outside the reinforced stir-zone, b-e) interface of stir-zone and TMAZ, f-g) inside the stir zone

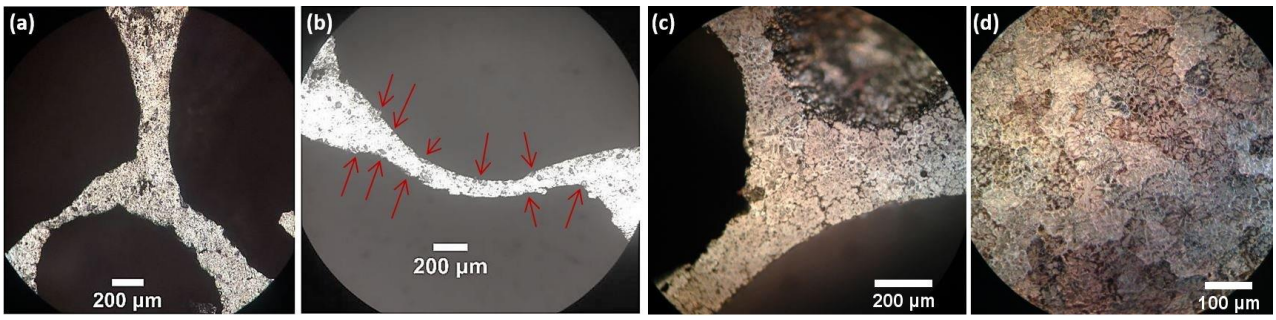

Figure 10. Interpore microstructure and texture evolution of ligaments: a) white field optical microscopy image, b) dark field optical microscopy image (red arrows indicate particles protruding on the solid-air interfaces of the foam cells), c - d) white field optical microscopy images of etched specimens

Figure 8b illustrates the variations of hardness distribution along the foamed (at its peak - 150 seconds) specimen. Outside the foamed stir-zone the microhardness distribution presented values in the range of 50-52 HV; whilst inside the foamed stir-zone the microhardness fluctuated from 68 to 71 HV. The decrease of the values in the foamed specimen corresponding to the precursor is caused by the intense grain growth (Figure 10d) and the elimination of the dislocations (which were created after strain hardening, H111) during the foaming process.

4. CONCLUSION

In the present work, a very promising method of manufacturing localized AA5083 – silicon carbide composite foam using Friction Stir Process was presented and the following concluding remarks can be drawn:

- Using friction stir process route, scope production of localized composite metal foam was successfully accomplished
- The optimum foaming efficiency resulted from three FSP passes (minimum) and the lower volume groove geometry.
- The higher volume groove geometry resulted in a non-uniform stabilizing particle (SiC) distribution in the precursor and this led to a higher collapsing rate during the foaming stage.
- The hardness measurements indicated a decrease in the values of the foamed specimen, corresponding the precursor specimen, which is attributed mainly to the intense grain growth during the foaming stage. Furthermore, the values inside the precursor and the foamed specimen stir-zones presented higher values in comparison to the areas outside the stir-zone.

Conclusively, the main novelty of the suggested method stems from the fact that foam structures can be obtained in different regions of the same metallic plate. The porosity, as well as the mechanical properties of the foamed structure can be controlled by the nature and the volume fraction of the foaming and the stabilization/reinforcing agent.

ACKNOWLEDGEMENTS

Prof. N.M. Vaxevanidis acknowledges financial support for the dissemination of this work from the *Special Account for Research of ASPETE* through the funding program "*Strengthening ASPETE's research*".

REFERENCES

[1] L. Gibson, M. Ashby: *Cellular Solids, Structure and Properties*, 2nd ed., Cambridge University Press, Cambridge, UK, 1997.

[2] M. Ashby, A. Evans, N. Fleck, L. Gibson, J. Hutchinson, H. Wadley: *Metal Foams: A Design Guide*, Butterworth-Heinemann, USA, 2000.

[3] B. Smith, S. Szyniszewski, J. Hajjar, B. Schafer, S. Arwade: Steel foam for structures: A review of applications, manufacturing and material properties, Journal of Constructional Steel Research, Vol. 71, pp. 1-10, 2012.

[4] B.A. Gama, T.A. Bogetti, B.K. Fink, C.J. Yue, D.T. Claar, H.H. Eiferte, J.W. Gillespie: Aluminum foam integral armor: a new dimension in armor design, Compos Struct, Vol. 52, pp. 381-395, 2001.

[5] J. Banhart: Manufacture, characterization and application of cellular metals and metal foams, Progr Mater Sci, Vol. 46, pp. 559-632, 2001.

[6] A.P. Mouritz, E. Gellert, P. Burchill, K. Challis: Review of advanced composite structures for naval ships and submarines, Compos Struct, Vol. 53, pp. 21-42, 2001.

[7] R.S. Mishra, Z.Y. Ma: Friction stir welding and processing, Mater Sci Eng R, Vol. 50, pp. 1-78, 2005.

[8] Z.Y. Ma: Friction Stir Processing Technology: A Review, Metall Mater Trans, Vol. 39A, pp. 642-658, 2008.

[9] D.J. Shindo, A.R. Rivera, L.E. Murr: Shape optimization for tool wear in the friction-stir welding of cast Al359-20% SiC MMC, J Mater Sci, Vol. 37, pp. 4999-5005, 2002.

[10] M. Yang, C. Xu, C. Wu: Fabrication of AA6061/Al2O3 nano ceramic particle reinforced composite coating by using friction stir processing, J Mater Sci, Vol 45, pp. 4431-4438, 2010.

[11] D.I. Pantelis, P.N. Karakizis, N.M. Daniolos, C.A. Charitidis, E.P Koumoulos, D.A. Dragatogiannis: Microstructural study and mechanical properties of dissimilar friction stir welded AA5083-H111 and AA6082-T6 reinforced with SiC nanoparticles, Mat Man Proc, Vol 31, pp. 264-274, 2016.

[12] Y. Hangai, T. Utsunomiya: Fabrication of Porous Aluminum by Friction Stir Processing, Metall Mater Trans, Vol. 40A, pp. 275-277, 2009.

[13] Y. Hangai, T. Utsunomiya, M. Hasegawa: Effect of tool rotating rate on foaming properties of porous aluminum fabricated by using friction stir processing, J Materials Proc Tech, Vol. 210, pp. 288-292, 2010.

[14] I. Papantoniou, E. Kyriakopoulou, D. Pantelis, A. Athanasiou-Ioannou, D. Manolakos: Manufacturing process of AA5083/nano-γAl2O3 localized composite metal foam fabricated by friction stir processing route (FSP) and microstructural characterization, Journal of Materials Science, Vol. 53, pp. 3817-3835, 2018.

[15] I. Papantoniou, H. Kyriakopoulou, D. Pantelis, D. Manolakos: Fabrication of MWCNT-reinforced Al composite local foams using friction stir processing route, Int J Adv Manuf Technol, Vol. 53, pp. 3817-3835, 2018.

[16] J. Hashim, L. Looney, M.S.J. Hashmi: The wettability of SiC particles by molten aluminium alloy, Journal of Materials Processing Technology, Vol. 119, pp. 324-328, 2001.

[17] D. Storjohann, O. Barabash, S. David, P. Sklad, E. Bloom, S. Babu: Fusion and friction stir welding of aluminium metal matrix composites, Metall Mater Trans, Vol. 36A, pp. 3237-3247, 2005.